

A Small-Molecule Antagonist of HIF2 α Is Efficacious in Preclinical Models of Renal Cell Carcinoma

Eli M. Wallace, James P. Rizzi, Guangzhou Han, Paul M. Wehn, Zhaodan Cao, Xinlin Du, Tzuling Cheng, Robert M. Czerwinski, Darryl D. Dixon, Barry S. Goggin, Jonas A. Grina, Megan M. Halfmann, Melissa A. Maddie, Sarah R. Olive, Stephen T. Schlachter, Huiling Tan, Bin Wang, Keshi Wang, Shanhai Xie, Rui Xu, Hanbiao Yang, and John A. Josey

Abstract

More than 90% of clear cell renal cell carcinomas (ccRCC) exhibit inactivation of the von Hippel-Lindau (pVHL) tumor suppressor, establishing it as the major underlying cause of this malignancy. pVHL inactivation results in stabilization of the hypoxia-inducible transcription factors, HIF1 α and HIF2 α , leading to expression of a genetic program essential for the initiation and progression of ccRCC. Herein, we describe the potent, selective, and orally active small-molecule inhibitor PT2385 as a specific antagonist of HIF2 α that allosterically blocks its dimerization with the HIF1 α /2 α transcriptional dimerization partner ARNT/HIF1 β . PT2385 inhibited the

expression of HIF2 α -dependent genes, including VEGF-A, PAI-1, and cyclin D1 in ccRCC cell lines and tumor xenografts. Treatment of tumor-bearing mice with PT2385 caused dramatic tumor regressions, validating HIF2 α as a pivotal oncogenic driver in ccRCC. Notably, unlike other anticancer agents that inhibit VEGF receptor signaling, PT2385 exhibited no adverse effect on cardiovascular performance. Thus, PT2385 represents a novel class of therapeutics for the treatment of RCC with potent preclinical efficacy as well as improved tolerability relative to current agents that target the VEGF pathway. *Cancer Res*; 76(18); 5491–500. ©2016 AACR.

Introduction

Aberrant activation of transcription factors is frequently associated with pathophysiologic conditions, including cancer. Transcription factors typically complex with other proteins and regulate gene transcription by binding to specific DNA sequences. As such, with the exception of nuclear hormone receptors, this class of proteins has been perceived as intractable targets for pharmacologic intervention. HIF2 α is one such protein that has been implicated in the initiation and progression of kidney cancer.

Nearly 64,000 new cases of kidney cancer were diagnosed in the United States in 2014, with approximately 70% being clear cell renal cell carcinoma (ccRCC; ref. 1). Patients with advanced disease are currently treated with antiangiogenesis agents, such as multitargeted tyrosine kinase inhibitors and specific VEGF

antagonists, inhibitors of mTOR, and immunomodulatory agents, such as inhibitors of PD-1. Few patients experience a complete response to these agents, and nearly all tumors progress during treatment (2). For patients with advanced or metastatic ccRCC, the 5-year survival rate is only 8% (1). It is thus clear that better therapeutic options are needed.

The HIF α family of transcription factors consists of HIF1 α , HIF2 α , and the less well characterized HIF3 α (3–5). Under hypoxic conditions, HIF α proteins accumulate and translocate to the nucleus, where they dimerize with ARNT. The HIF α -ARNT heterodimers bind to the hypoxia-responsive elements (HRE) on target genes whose products coordinately regulate anaerobic metabolism, angiogenesis, cell proliferation and survival, extracellular matrix remodeling, pH homeostasis, amino acid and nucleotide metabolism, and genome stability (6–8). Under normoxic conditions, specific proline residues on the HIF α proteins are hydroxylated by the dioxygenase HIF-specific prolyl-hydroxylases (9, 10). These posttranslational modifications serve as recognition sites for the von Hippel-Lindau (pVHL) tumor suppressor protein, which binds to the hydroxylated proline residues as part of an E3 ubiquitin-ligase complex that then targets HIF α proteins for proteasomal degradation.

In more than 90% of ccRCC patients, pVHL is defective, caused by gene deletion, mutation, epigenetic silencing, or posttranslational modifications (11), resulting in the stabilization of HIF α proteins. Over the last decade, accumulating data have suggested an oncogenic role for HIF2 α in pVHL-defective ccRCC. In pVHL-defective ccRCC xenografts, knockdown of HIF2 α expression inhibits tumor formation comparable with reintroduction of functional *VHL*, and overexpression of a stabilized variant of

Peloton Therapeutics, Inc., Dallas, Texas.

Note: Supplementary data for this article are available at Cancer Research Online (<http://cancerres.aacrjournals.org/>).

Current address for D.D. Dixon: Bristol-Myers Squibb, New Brunswick, New Jersey; current address for M.M. Halfmann: Stowers Institute for Medical Research, Kansas City, Missouri; current address for M.A. Maddie: Renovo Neural, Inc., Cleveland, Ohio; and current address for S.R. Olive: Progen Lab, Dallas, Texas.

Corresponding Author: Eli M. Wallace, Peloton Therapeutics Inc., 2330 Inwood Road, Suite 226, Dallas, TX 75235. Phone: 972-629-4126; Fax: 972-629-4111; E-mail: eli.wallace@pelotontx.com

doi: 10.1158/0008-5472.CAN-16-0473

©2016 American Association for Cancer Research.

HIF2 α alone is sufficient to overcome the tumor-suppressive effect of pVHL (12–15). In contrast, HIF1 α is often deleted or mutated in ccRCC, and overexpression of HIF1 α inhibited tumor growth in pVHL-defective xenografts (12, 16, 17). These data suggest that HIF2 α may be the tumorigenic driver in ccRCC and highlight the therapeutic potential of HIF2 α antagonists for its treatment.

Biophysical studies have revealed a hydrophobic pocket in the HIF2 α PAS-B domain, leading to the discovery of a small molecule that binds within the pocket and allosterically disrupts HIF2 α dimerization to ARNT (18–19). Although this early work was seminal in identifying the possibility of antagonizing this transcription factor, the reported antagonists exhibit modest cellular potency and, most importantly, poor physical properties that preclude their use in validating HIF2 α as a target for treatment of ccRCC. Guided by iterative structure-based design utilizing the heterodimer of PAS-B domains of HIF2 α and ARNT, we have discovered potent HIF2 α antagonists with excellent pharmacologic properties, thereby enabling *in vivo* evaluation of this novel anticancer mechanism. Here, we describe PT2385 [(S)-3-((2,2-difluoro-1-hydroxy-7-(methylsulfonyl)-2,3-dihydro-1H-inden-

4-yl)oxy)-5-fluorobenzonitrile] (Fig. 1A), a HIF2 α antagonist with potent antitumor activity. We also propose a mechanism by which this molecule inhibits HIF2 α transcriptional activity.

Materials and Methods

Crystallography of HIF2 α -B α :ARNT-B α complex

The preparation of HIF2 α -B α :ARNT-B α complex was described previously (20). The crystals of the heterodimer were produced by hanging drop vapor diffusion. The well solution contained 16% PEG 3350 and 50 mmol/L BisTris, pH 5.4, and the crystallization drop was obtained by mixing 1 μ L of well solution and 1 μ L of heterodimer at 12 mg/mL in 20 mmol/L Tris-HCl, pH 8.0, and 1 mmol/L DTT. Right after the mixing, crystal seeds from crushed old crystals were transferred to the drop with a whisker. Diffraction quality crystals typically grew after 2 or 3 days. For soaking, 5 μ L of the soaking solution, which consisted of 1 mmol/L PT2385, 20% PEG 3350, 5% DMSO, and 50 mmol/L Bis-Tris, pH 5.4, was added to a crystal drop. Typically, soaking was carried out for 2 or 3 days before harvest. Freezing solution consisted of 1 mmol/L PT2385, 20% PEG 3350, 15% DMSO, and 50 mmol/L Bis-Tris,

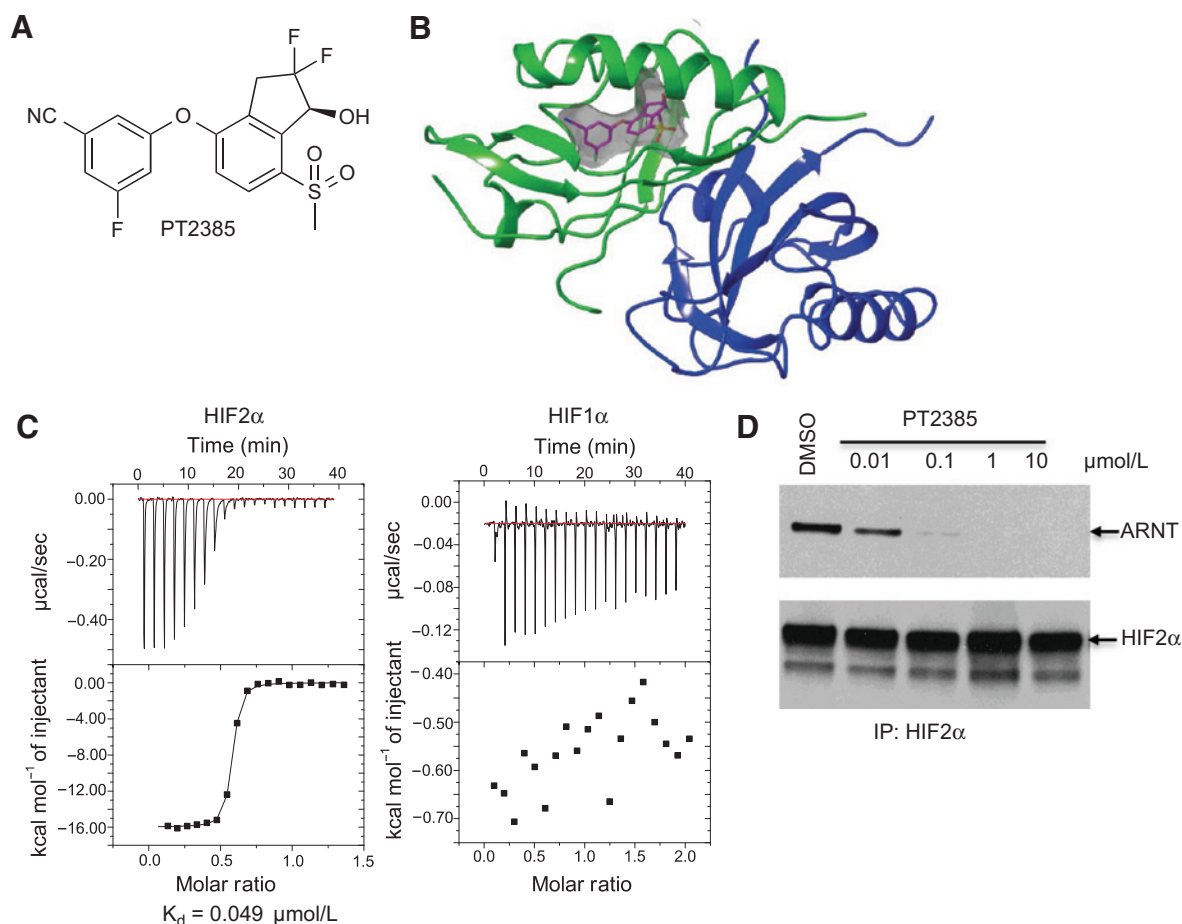


Figure 1.

Binding of PT2385 to HIF2 α PAS-B domain disrupts HIF2 α /ARNT dimer formation. **A**, chemical structure of PT2385. Synthetic procedures, scheme, and characterization of PT2385 are available in Supplementary Methods. **B**, ribbon diagram of co-crystal structure of HIF2 α PAS-B α domain (green), ARNT PAS-B α domain (blue), and PT2385 (magenta). **C**, binding affinity of PT2385 to PAS-B domains of human HIF2 α and HIF1 α using ITC. **D**, coimmunoprecipitation (IP) experiment in 786-O cells demonstrating PT2385 disrupts HIF2 α and ARNT dimerization.

pH 5.4. For harvest, crystals were briefly soaked in the freezing solution for a few seconds before they were flash frozen in liquid nitrogen. Diffraction data were collected at beam-line 19ID at Advanced Photon Source (Argonne National Laboratory). All data were indexed and scaled with program HKL2000 (21). Model building and refinement were carried out with COOT (22) and REFMACS (23), respectively.

Isothermal titration calorimetry

Human HIF2 α -B was expressed and purified as described earlier (20). Rat HIF2 α differs from human HIF2 α -B by only three amino acids. So, the expression vector for human HIF2 α -B was mutated at these residues (T262L, I 265V, and I326V) to make rat HIF2 α -B. Pas-B domain of HIF1 α was unstable, and the complex of HIF1 α -B*:ARNT-B* was used for isothermal titration calorimetry (ITC). The complex was coexpressed in *Escherichia coli* harboring pET28-HIF1 α -B* and pGB1-ARNT-B* and copurified in a single step of Ni-affinity chromatography. The binding affinity between PT2385 and PAS-B domains was determined using ITC on an iTC200 system (GE Healthcare). PAS-B at 0.4 mmol/L was titrated into 40 μ mol/L of PT2385 in the cell in buffer consisting of 20 mmol/L Tris-HCl, pH 8.0, 150 mmol/L KCl, and 1% DMSO.

Cell culture

786-O, A498, Hep3B, and Caki-1 cell lines were purchased from ATCC. All were acquired in 2012 and were maintained in culture for no more than 30 continuous passages. The cells were cultured in DMEM (D5796, Sigma) supplemented with 10% FBS (F6178, Sigma), 100 units penicillin, and 100 μ g/mL streptomycin (P4333, Sigma).

For compound treatment, 5×10^5 cells were plated into 6-well cell culture plates (Corning cat# 3506) in 2 mL of medium. Compound dissolved in DMSO was added as the cultures reached confluence with the final concentration of DMSO at 0.1%. For hypoxia-treated cells, cell cultures were placed in the chamber supplied with 1% oxygen and 5% CO₂ (COY Laboratory Products) for more than 4 hours before compound addition and maintained under the hypoxic condition for the duration of compound treatment.

All relevant human cell lines used in experiments were obtained from ATCC. ATCC authenticated cell lines with short tandem repeat profiling.

Coimmunoprecipitation of HIF α and ARNT

Cells in 6-well plate were lysed in 1 mL of cell lysis buffer (Tris-HCl 20 mmol/L, pH 7.5, Triton X-100 1%, NaCl 150 mmol/L, glycerol 5%, EDTA 1 mmol/L, DTT 1 mmol/L, and 1 tablet per 10 mL of Roche Protease Inhibitor Tablet Complete). A total of 1 μ g of mouse mAb against human ARNT (Santa Cruz Biotechnology, sc-55526) or 1 μ g of antibody against HIF2 α (Abcam Ab199) and 50 μ L of Protein AG Beads (Santa Cruz Biotechnology 50% slurry in lysis buffer) were added to cleared cell lysate. The tubes were rotated at 4°C for 16 hours. After washing in cold lysis buffer, the bead-bound proteins were separated by SDS gel electrophoresis and subjected to Western blotting with specific antibodies.

RNA preparation and quantitative RT-PCR

Total RNA was prepared using Direct-zol™ RNA Miniprep Kit from Zymo Research Corp (cat 2053). Total RNA (2 μ g) was used to make single-stranded cDNA in 100 μ L reaction containing

20 μ L of 5 \times buffer (supplied with the Superscript II enzyme), 10 mmol/L of DTT, 200 units of Superscript II (Life Technologies, cat 18064014), 0.5 mmol/L of dNTP mix (Promega, cat U1515), and 40 μ g/mL random hexamer primers (Roche, cat 11034731001) using the following thermocycler program: 25°C for 10 minutes, 42°C for 50 minutes, and then 72°C for 10 minutes. A total of 1.25 μ L of the resulting cDNA was used in each quantitative PCR reaction in A&B Applied Biosystem ViiA 7 equipment using SYBR Select Master Mix or TaqMan Mix supplied by A&B Applied Biosystem (cat 4472913). Each sample was run in triplicate. The expression of specific genes was normalized against cyclophilin.

The primer sequences used for quantitative RT-PCR are as follows:

hEpo-F GGAGCCGAGAATATCACGAC
 hEpo-R CCCTGCCAGACTTCTACGG
 hSerpine1 (PAI-1)-F ACCGCAACGTGTTTCTCA
 hSerpine1 (PAI-1)-R TTGAATCCCATAGCTGCTTGAAT
 hPGK1-F TAAAGGGAGCCGGTCTGTTA
 hPGK1-R TCCATTGTCCAAGCAGAATTTGA
 hPDK1-F GAACCCAAAGACATGACGACG
 hPDK1-R ATGTCCCAAGTGTGTCTAGGCA
 hCyclinD1-F TGGAGCCCGTGAAAAAGAGC
 hCyclinD1-R TCTCCTTCATCTTAGAGCCAC
 hGLUT1-F TCTGGCATCAACGCTGTCTTC
 hGLUT1-R CGATACCGGAGCCAATGGT
 hHIF2 α -F GCGACAATGACAGCTGACAA
 hHIF2 α -R CAGCATCCCCGGGACTTCT
 hCyclophilin-F TGCCATCGCCAAGGAGTAG
 hCyclophilin-R TGCACAGACGGTCACTCAA

Cell proliferation assay

A498 cells (2×10^3) and 786-O cells (1×10^4) were seeded in 96-well plates. PT2385 was added to the plates 24 hours after seeding. After 72 hours, thiazolyl blue tetrazolium bromide (MTT, Sigma) was added to the final concentration of 0.5 mg/mL. Four hours later, cell culture media were removed by aspiration, and 100 μ L of DMSO was added to each well. After shaking for 10 minutes, optical density was read at 570 nm with a reference filter at 650 nm on a Biotek Synergy.

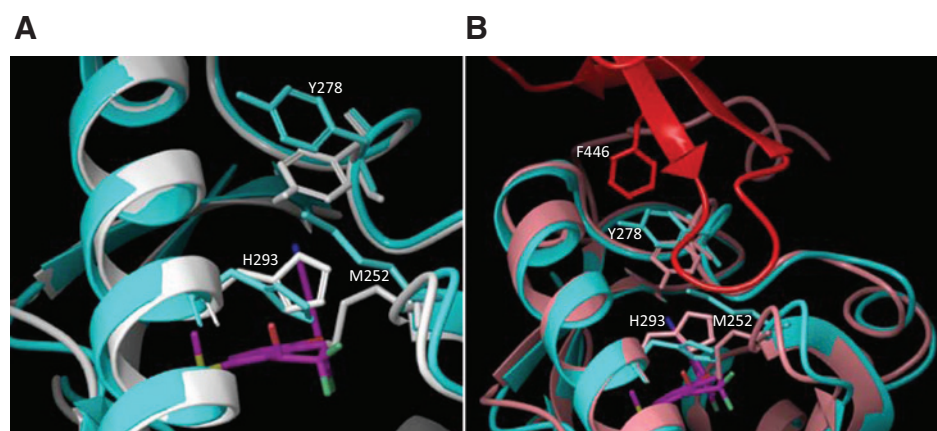
IHC

Tumor samples were fixed in 10% formalin for 24 hours then stored in 70% alcohol.

Sample processing, embedding, and sectioning were performed by HistoTox Labs, Inc. IHC for Ki67 and active caspase-3 was performed by HistoTox Labs, Inc. IHC for CD31 was performed by Reveal Biosciences LLC. IHC for HIF2 α was performed using mAb (Santa Cruz Biotechnology, sc46691) with 1:500 dilution. The slides were viewed with Nikon Eclipse Ci system, and the images were captured with a Nikon DS-Fi2 imaging system.

Mouse pharmacokinetics of PT2385

PT2385 was suspended in 0.5% methylcellulose, 0.5% Tween 80 in water (w/v) to yield a suspension with concentrations of 3, 10, and 30 mg/mL, respectively. The dosing volume was 10 mL/kg. Mice were dosed by oral gavage. Blood samples were taken at 0.25, 0.5, 1, 2, 4, 8, 12, and 24 hours postdose from 3 mice per time point. Plasma PT2385 concentration was determined by LC/MS-MS system (Agilent Technologies).

**Figure 2.**

PT2385 induces specific perturbations of HIF2 α PAS-B* domain residues H293, M252, and Y278. **A**, superimposition of HIF2 α PAS-B* apo structure (white) with HIF2 α PAS-B* co-crystal structure (cyan) containing PT2385 (magenta). **B**, superimposition of HLH HIF2 α (pink)/ARNT (red) with PAS-B* co-crystal structure (cyan) containing PT2385 (magenta).

Mouse xenograft models and PT2385 treatment

The protocol and procedures involving the care and use of animals for this study were reviewed and approved by the Institutional Animal Care and Use Committee of University of Texas Southwestern Medical Center (Dallas, TX). A total of 4×10^6 RCC cells in a volume of 100 μ l of PBS and Matrigel (1:1 in volume) were inoculated subcutaneously in the rear right flanks of SCID/Beige mice of 6 to 7 weeks of age for xenograft development. For the PDX xenograft model, tumor fragments harvested from donor animals at passage 7 were implanted in the flank region of female NCr nude mice (Taconic) of 5 to 8 weeks of age. Tumor size and body weight were measured twice a week.

PT2385 was formulated with 10% absolute ethanol, 30% PEG400, 60% water containing 0.5% methylcellulose and 0.5% Tween 80, and was administered to mice by gavage.

Plasma human and mouse VEGF-A measurements

The plasma levels of human and mouse VEGF-A were measured with the human (catalog #: DVE00) or mouse (catalog #: MMV00) Quantikine VEGF ELISA Kits from The D&D Systems by following the manufacturer's instructions.

Cardiovascular effect evaluation

The study was performed by CorDynamics, Inc. Briefly, telemetered male Sprague–Dawley rats were treated with PT2385 at 30 or 100 mg/kg twice daily, or sunitinib at 40 mg/kg once daily for 5 consecutive days. Systemic blood pressure (SAP, DAP, MAP), HR, pulse pressure, and ECG parameters (PR interval, QRS duration) were recorded from predose to 24 hours after the final dose and were reported in hourly averages.

Results

Binding and dimerization disruption

Protein co-crystal structure elucidation using HIF2 α /ARNT PAS-B* domains demonstrates that PT2385 binds to a fully enclosed lipophilic cavity in the recombinant PAS-B* domain of HIF2 α (Fig. 1B; refs. 20, 24). The K_d for this PT2385–HIF2 α PAS-B interaction is approximately 50 nmol/L as measured by ITC (Fig. 1C). Under the same experimental condition, ITC reveals no binding of PT2385 to the PAS-B domain of HIF1 α .

Disruption of the full-length HIF2 α /ARNT interaction was assessed by coimmunoprecipitation assay in 786-O cells, a VHL-mutant ccRCC cell line with constitutively active HIF2 α and no functional HIF1 α due to the truncation of the *Hif1 α* gene.

HIF2 α is immunoprecipitated from lysates of 786-O cells treated with PT2385. Immunoblotting shows that ARNT protein coprecipitating with HIF2 α is diminished in response to PT2385 treatment in a dose-dependent manner, indicating that the compound disrupts HIF2 α /ARNT dimer formation (Fig. 1D).

Structural comparison of PT2385-bound HIF2 α /ARNT PAS-B* domains and free (apo) PAS-B* domains indicates that compound binding did not perturb the beta-sheet interface of the two PAS-B* domains but did cause significant changes to residues H293, M252, and Y278 on the opposite face of the beta-sheet floor (Fig. 2A).

Examination of the recently reported crystal structure of the more complete helix-loop-helix: PAS-A: PAS-B (HLH-A-B) heterodimer of HIF2 α and ARNT reveals that the HIF2 α /ARNT PAS-B* domains occupy a completely different spatial arrangement and dimer interface (25). In this orientation, the perturbed residues now reside at the HIF2 α /ARNT PAS-B interface, suggesting that PT2385-induced changes to residues H293, M252, and Y278 are responsible for dimer disruption (Fig. 2B).

Inhibition of HIF2 α transcriptional program

PT2385 inhibition of HIF2 α transcriptional activity in cells was evaluated by qPCR quantitation of known HIF2 α target gene transcripts. Treatment of 786-O cells with PT2385 significantly reduces the levels of mRNA for *CCND1*, *VEGF-A*, *GLUT1*, and *PAI-1* in a concentration-dependent manner (Fig. 3A). The specificity of PT2385 was further evaluated in Hep3B hepatoma cells, which accumulate both HIF1 α and HIF2 α proteins under hypoxia and where HIF α -specific gene regulation has been previously delineated. Treatment of Hep3B cells with PT2385 reduces hypoxia-induced expression of erythropoietin (*EPO*) and *PAI-1*, both known HIF2 α target genes (26–28). Compound treatment has no effect on expression of either *PGK1* or pyruvate dehydrogenase kinase 1 (*PDK1*) genes, which are specifically regulated by HIF1 α in Hep3B cells (Fig. 3B; refs. 29, 30). Consistent with the gene expression data, PT2385 only disrupts HIF2 α , but not HIF1 α , heterodimerization with ARNT in Hep3B cells (Fig. 3C).

PT2385 has no effect on the proliferation or viability of 786-O and A498 cells in culture at concentration as high as 10 μ mol/L (Supplementary Fig. S1). This result is consistent with the observations that shRNA- or siRNA-mediated HIF2 α knockdown does not affect cell proliferation *in vitro* (14, 15). Collectively, the *in vitro* data indicate that PT2385 is a potent and highly selective inhibitor of HIF2 α -dependent gene expression.

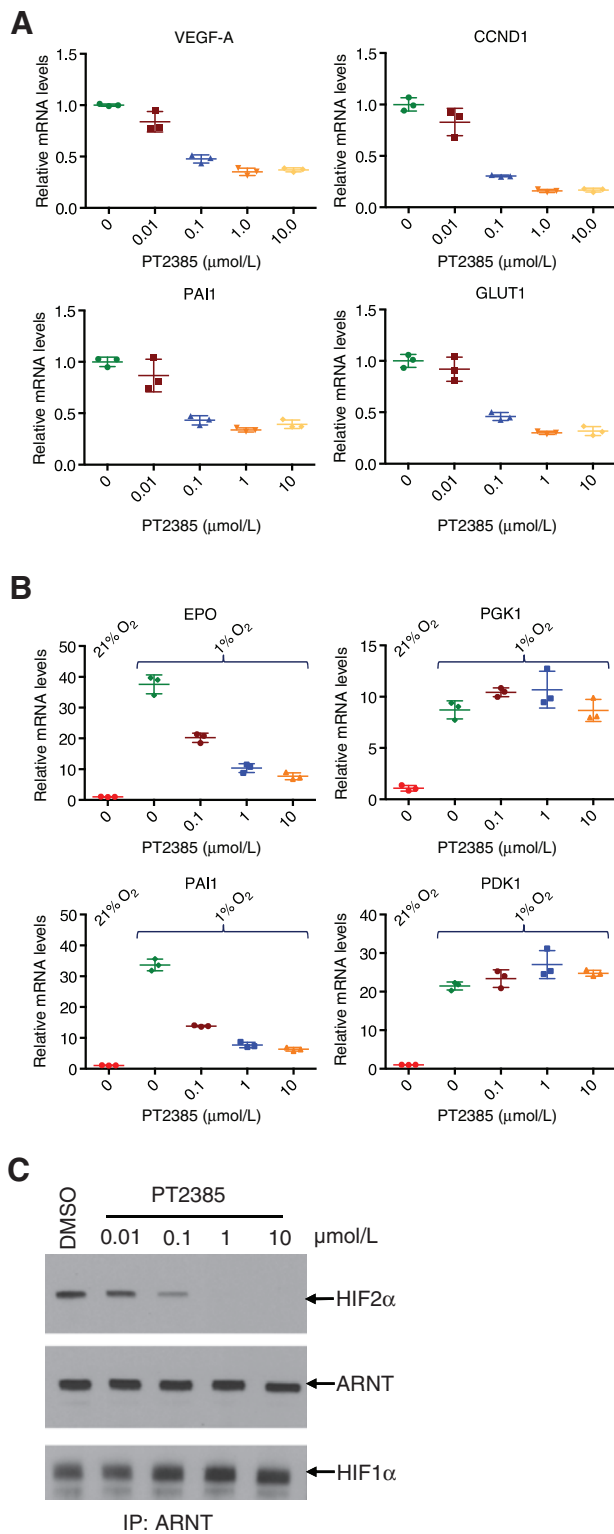


Figure 3. PT2385 inhibits HIF2 α target gene transcription and is selective for HIF2 α . **A**, PT2385 treatment inhibits HIF2 α target gene expression in 786-O cells. **B**, PT2385 does not inhibit HIF1 α target gene expression in hypoxic Hep3B cells. **C**, PT2385 does not disrupt HIF1 α /ARNT dimer formation in hypoxic Hep3B cells. IP, immunoprecipitation.

Pharmacologic activity of PT2385

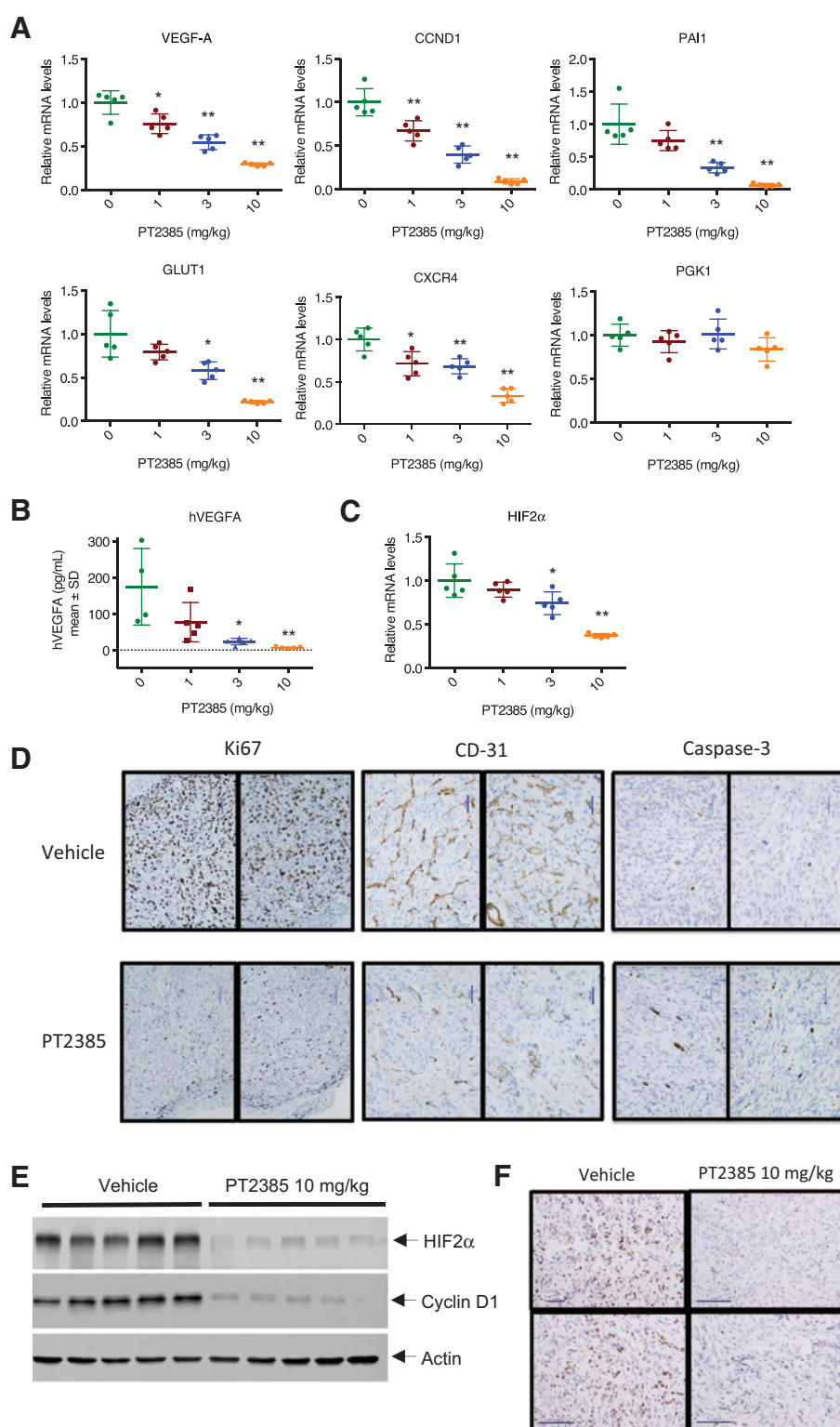
High plasma levels of PT2385 are achieved by oral dosing in mice, which enables the evaluation of compound effect on gene expression in xenograft tumor models (Supplementary Fig. S2). SCID/beige mice with established 786-O tumors were treated with six doses of PT2385 at 12-hour intervals. Tumors were excised 12 hours after the last dose for RNA analysis. Serum samples were collected for the measurement of human VEGF-A. Expression of HIF2 α target genes *VEGF-A*, *CCND1*, *PAI1*, *GLUT1*, and *CXCR4* is inhibited in a dose-dependent manner, whereas the expression of the non-HIF2 α target gene *PGK1* remains unchanged even at the highest dose (10 mg/kg; Fig. 4A). Consistent with the mRNA data, circulating tumor-derived human VEGF-A and tumor protein cyclin D1 levels are significantly reduced in response to PT2385 treatment (Fig. 4B and E). Similarly, in the A498 xenograft model, PT2385 treatment (10 mg/kg) inhibited the expression of HIF2 α target genes *VEGF-A*, *CCND1*, and *CXCR4*, as well as circulating tumor-derived human VEGF-A levels (Supplementary Fig. S3). Immunohistochemical staining of tumor tissue sections reveals significant reduction of Ki67 and CD31, markers of cell proliferation and of angiogenesis, respectively, in tumors from mice treated with PT2385. Staining of activated caspase-3 shows an increase in positive cells in PT2385-treated tumors, consistent with an increase in tumor cell apoptosis (Fig. 4C).

Unexpectedly, PT2385 also reduced HIF2 α mRNA and protein levels in xenograft tumors, an effect that was not observed in 786-O cells in culture (Fig. 4D–F and Supplementary Figs. S3 and S4). This observation raised the possibility that HIF2 α might regulate the transcription of its own gene in the xenograft tumors and is consistent with a report that overexpression of HIF2 α protein enhances *EPAS1* gene promoter activity (31). These findings are also consistent with the observation that HIF2 α mRNA levels were elevated in ccRCC tumors with *VHL* mutations (32).

Antitumor activity in ccRCC models

Tumor xenografts were established in the flanks of SCID/beige mice with the 786-O and A498 RCC cell lines. When tumor size reached 200 to 300 mm³, the mice were administered PT2385 by oral gavage at indicated doses on a daily basis. In the 786-O xenograft model, both 3 and 10 mg/kg PT2385 given twice daily result in a rapid, dose-dependent tumor regression. In contrast, a multi-tyrosine kinase inhibitor, sunitinib, at 40 mg/kg given once daily produces only tumor stasis (Fig. 5A and B). In the A498 xenograft model, PT2385 induces tumor stasis at 6 mg/kg once daily and tumor regression at 20 and 60 mg/kg once daily. Sunitinib at 40 mg/kg once daily has a similar effect as the higher doses of PT2385 (Fig. 5C and D).

We further evaluated the antitumor efficacy of PT2385 in a patient-derived xenograft (PDX) model. The ccRCC tumor is *VHL* deficient, expresses both HIF1 α and HIF2 α (Supplementary Fig. S5), and is derived from a patient that progressed after treatment with sunitinib and everolimus. Tumor-bearing mice were treated with 30 mg/kg of PT2385 twice daily or 40 mg/kg of sunitinib once daily. After 4 weeks, PT2385 treatment completely inhibited tumor growth, whereas sunitinib had no impact (Fig. 5E). These data indicate that PT2385 has efficacy in *VHL*-mutant ccRCC tumors that express both HIF1 α and HIF2 α proteins. Furthermore, PT2385 demonstrated superior efficacy to sunitinib in 2 of 3 models evaluated, supporting that HIF2 α antagonism has broad antitumor effects beyond

**Figure 4.**

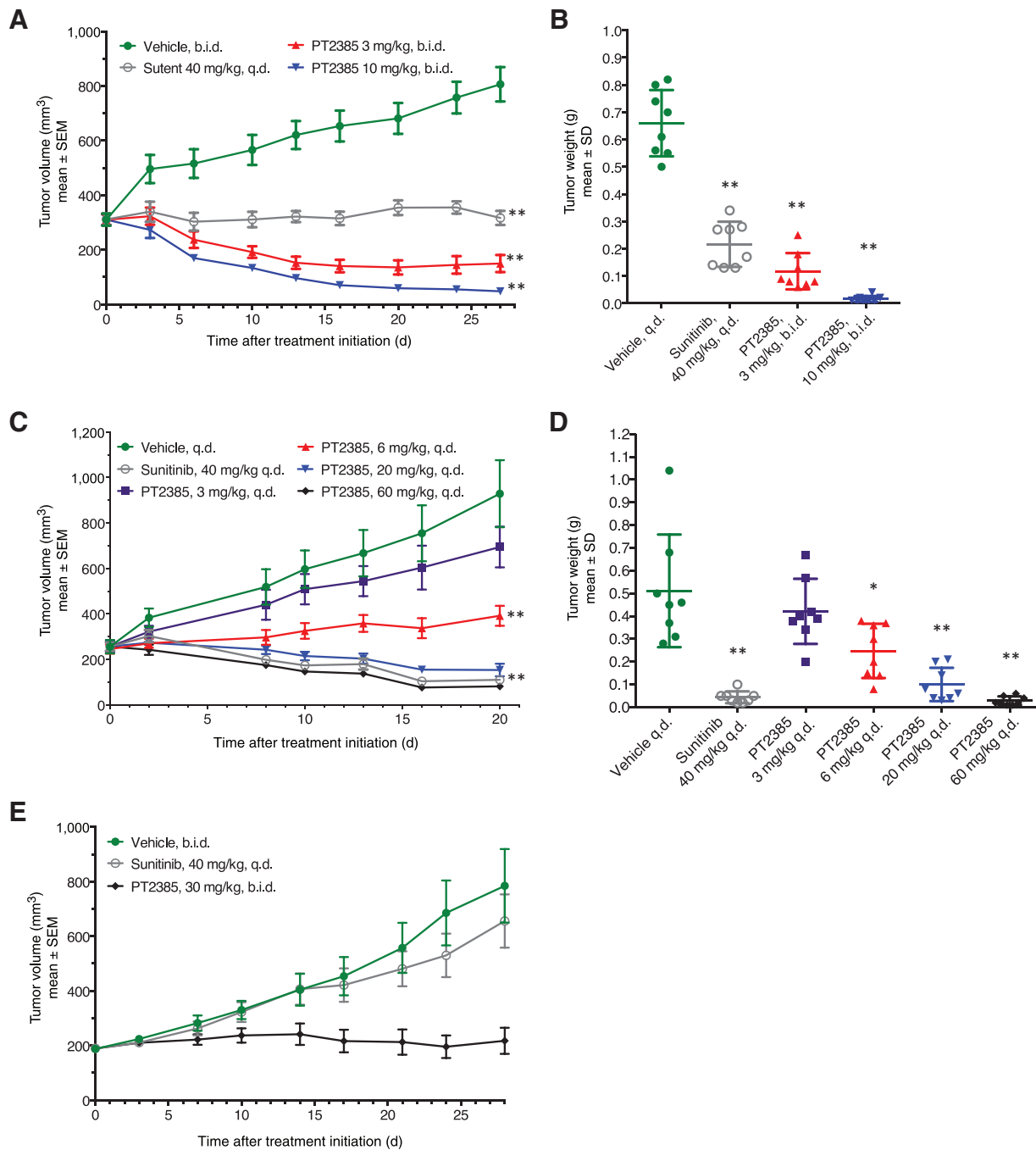
Pharmacologic activity of PT2385. 786-O tumor-bearing mice received six oral doses of PT2385 on twice daily schedule. Twelve hours after the last dose, tumors were excised. **A**, the levels of mRNA for HIF2 α -regulated genes *VEGF-A*, *CCND1*, *GLUT1*, *PAI1*, and *CXCR4* were decreased. The mRNA levels of non-HIF2 α target gene *PGK* did not change. **B**, circulating human VEGF-A levels were reduced.

*, $P < 0.05$; **, $P < 0.01$ (unpaired t test comparing treated group with vehicle control group). **C**, qRT-PCR indicates reduction of HIF2 α mRNA in response to PT2385 treatment. **D**, IHC indicates decreased Ki67 AND CD31 and increased active caspase-3 in tumors. Each image is from an individual tumor. **E**, immunoblotting shows reduction of HIF2 α and cyclin D1 proteins in tumors treated with PT2385 (five tumors from each of the control and treated groups). **F**, IHC indicates that PT2385 treatment reduces HIF2 α protein in tumors. Each image was from an individual tumor.

antiangiogenesis in ccRCC. PT2385 was well tolerated in all three models, with no weight loss or behavioral changes observed (Supplementary Fig. S6A–S6C).

Cardiovascular assessment of PT2385

Hypertension is a common side effect of antibodies and tyrosine kinase inhibitors that target VEGF/VEGFR2 signaling

**Figure 5.**

Antitumor activity of PT2385 in ccRCC models. Daily PT2385 or sunitinib treatment was initiated when the flank xenograft tumor reached 200 to 300 mm³ for **A–E**. **A**, PT2385 inhibits tumor growth in 786-O xenograft model ($n = 8$). q.d., once daily; b.i.d., twice daily. **B**, PT2385 reduces tumor weight in 786-O xenograft model ($n = 8$). **C**, PT2385 inhibits tumor growth in A498 xenograft model ($n = 8$). **D**, PT2385 reduces tumor weight in A498 xenograft model ($n = 8$). **E**, PT2385 inhibits tumor growth in a patient-derived ccRCC xenograft model ($n = 8$). *, $P < 0.05$; **, $P < 0.01$ (unpaired t test comparing treated group with vehicle control group).

(33–35). As PT2385 inhibits VEGF-A production in tumor cells, it is of interest to examine whether it elicits hemodynamic effects in a rodent model (36). Naïve telemetered male Sprague–Dawley rats were treated with PT2385 or sunitinib for 5 days. Systemic

blood pressure, heart rate, pulse pressure, and ECG parameters were recorded and reported hourly for the entire duration of the dosing regimen. At either dose tested, PT2385 does not have any detectable effect on any hemodynamic or electrocardiographic

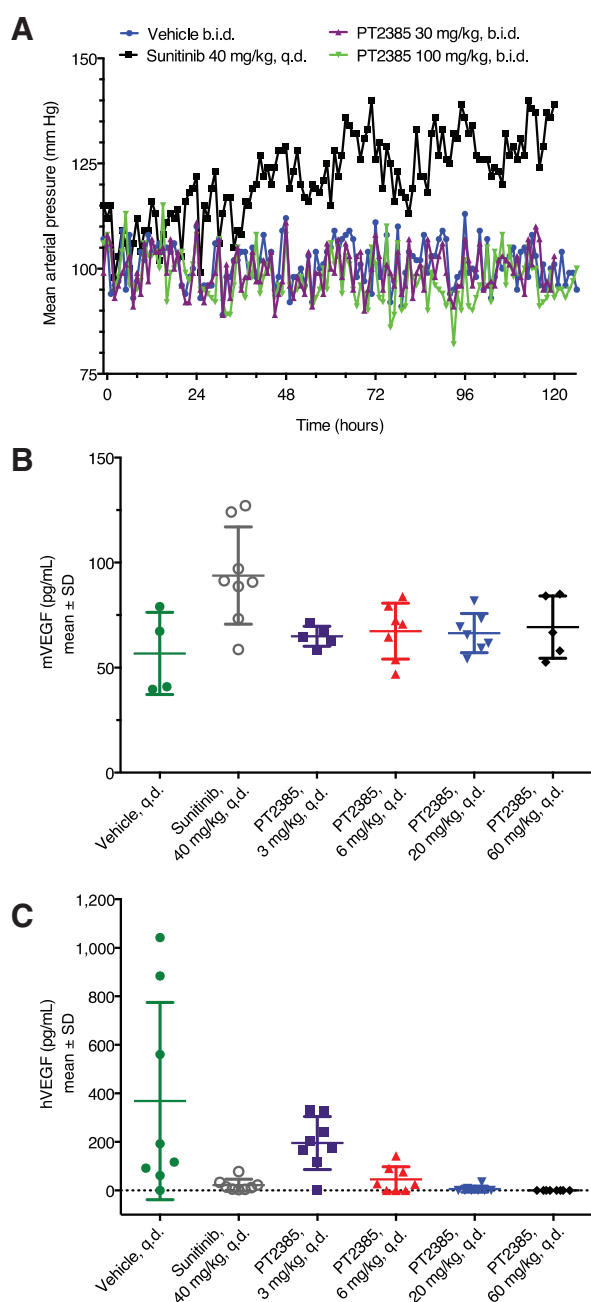


Figure 6.

Impact of PT2385 on blood pressure and host VEGF-A expression. **A**, telemetered rats were treated with PT2385 or sunitinib for 5 consecutive days. q.d., once daily; b.i.d., twice daily. Mean arterial pressure was reported in hourly averages. Sunitinib caused a progressive increase of blood pressure, whereas PT2385 exerted no effect. **B**, PT2385 does not change the levels of circulating mouse VEGF-A in A498 xenograft tumor-bearing mice after 24 days of treatment, whereas it significantly reduced tumor-derived human VEGF-A. *, $P < 0.05$ (unpaired t test comparing treated group with vehicle control group).

parameters. In contrast, administration of sunitinib results in a progressive increase in systemic arterial blood pressure (Fig. 6A). There were no notable changes in pulse pressure or ECG parameters observed in rats treated with either compound.

We further examined whether PT2385 altered host VEGF-A production in tumor-bearing mice. SCID/beige mice bearing A498 xenograft tumors were treated with PT2385 for 24 days. Serum mouse and human VEGF-A levels were determined 12 hours after the final dose (trough drug concentrations). PT2385 does not reduce circulating mouse VEGF-A but reduces tumor-derived human VEGF-A levels (Fig. 6B and C). The lack of effect on mouse VEGF-A is not due to species selectivity of PT2385 in antagonizing HIF2 α . The compound inhibits rodent HIF2 α as it binds to rat HIF2 α and reduces mouse *EPO* mRNA levels in the kidney (Supplementary Fig. S7A and S7B). A likely explanation for the lack of effect on host VEGF-A production is that unlike VEGF-A expression in the RCC tumors, host VEGF-A expression is regulated by other factors than HIF2 α .

Discussion

The oncogenic role of HIF α proteins in ccRCC is strongly implicated by human genetics. First, patients carrying germline mutations in the *VHL* gene are predisposed to ccRCC (37). Second, inactivation of pVHL due to somatic mutations and/or epigenetic modifications has been found in a majority of sporadic ccRCC tumors (8). pVHL deficiency leads to the stabilization of HIF α proteins, which enhance the expression of genes normally activated only when cells are under hypoxic stress. HIF α -activated gene products support cell survival and proliferation and, thus, can promote tumorigenesis. Although both HIF1 α and HIF2 α are stabilized as a result of pVHL deficiency, there is a preponderance of evidence in support of HIF2 α being the oncogenic driver for ccRCC (*vide supra*). For these reasons, HIF2 α has long been viewed as a potential target in the search for breakthrough treatments for ccRCC.

Using structure-based design employing the PAS-B* domains of HIF2 α and ARNT, we have discovered potent, selective, orally bioavailable HIF2 α antagonist PT2385. This discovery is noteworthy as PT2385 is a direct antagonist of a gene-specific transcription factor not of the nuclear hormone receptor family, thereby establishing binding to PAS-B domains as a viable mode for the discovery of novel transcription factor antagonists. Evaluation of available protein:inhibitor crystallographic data allows us to propose a mechanism for small-molecule inhibition of HIF2 α transcriptional activity with PT2385. The x-ray co-crystal structure of PT2385 with the PAS-B* domains of the HIF2 α /ARNT complex (Fig. 1B) shows that PT2385 is completely engulfed within HIF2 α . Although this structure reveals important points of interaction within the complex that enabled lead optimization and ultimately to the discovery of PT2385, it does not explain how PT2385 is able to allosterically disrupt the HIF2 α /ARNT dimer. In the PT2385-bound HIF2 α structure, the beta-sheet interface of the two PAS-B* domains show essentially no perturbations compared with the unbound (apo) structure. However, there are significant perturbations of HIF2 α residues H293, M252, and Y278 on the opposite face of the beta-sheet floor (Fig. 2A). The significance of these perturbations became apparent in light of a recently published crystal structure of the more complete HLH-A-B heterodimer of HIF2 α and ARNT, which revealed an alternative spatial arrangement and interface of the two PAS-B domains (25). Although the folds for both HIF2 α PAS-B domain structures are essentially identical, the domain arrangement of the HLH-A-B dimer revealed that the PT2385 perturbed amino acids are now located at the HIF2 α /ARNT PAS-B interface (Fig. 2B), suggesting

that they may be responsible for dimer disruption. In support of this argument, a mutation in ARNT (F466L) rendered a PDX tumor line resistant to dimer disruption by a structurally related HIF2 α inhibitor (J. Brugarolas, personal communication). In the apo structure, ARNT residue F466 is in very close proximity to HIF2 α Y278 (Fig. 2A). The binding of PT2385 creates a highly unfavorable van der Waals interaction between ARNT F466 and HIF2 α Y278 caused by the concerted movement of HIF2 α PAS-B residues H293 and M252. ARNT F466L mutation would alleviate the steric clash, allowing the dimer to remain intact. This mechanistic hypothesis suggests perturbation of a few amino acid residues within the PAS-B domain is sufficient to disrupt a large protein:protein interface leading to complete blockage of HIF2 α -driven gene transcription.

Using PT2385, we are able to evaluate the role of HIF2 α in ccRCC. HIF α proteins control a large battery of genes in a cell type- and cell context-dependent manner (8). In the current study, we observe strong inhibition of *VEGF-A*, *PAI-1*, *cyclin D1*, *CXCR4*, and *GLUT1* gene expression with PT2385 treatment and no effect on HIF1 α -controlled genes (Figs. 3A and B and 4A). Each of the genes regulated by PT2385 plays a unique role contributing to tumor growth or metastasis. Consistent with inhibition of multiple gene products involved in tumorigenesis, PT2385 exhibits strong antitumor activity, including a PDX model that expresses both HIF2 α and HIF1 α (Fig. 5E). In cell line xenografts that express high levels of HIF2 α , PT2385 treatment results in rapid regression of established tumors (Fig. 5A–D). IHC of tumor sections indicates that PT2385 treatment reduced angiogenesis, cell proliferation, and increased cell apoptosis (Fig. 4C), indicating that multiple mechanisms contribute to its antitumor activity.

PT2385 shows no effect on the proliferation of ccRCC tumor cell lines in culture, even though it inhibits HIF2 α target gene transcription (Fig. 3A and Supplementary Fig. S1). The lack of cytotoxicity of HIF2 α antagonism *in vitro* is consistent with previous studies showing shRNA-mediated HIF2 α knockdown does not affect cell survival and proliferation in culture but does inhibit xenograft tumor growth (14, 15). These results reinforce the conclusion that PT2385 inhibits tumor growth through selective inhibition of HIF2 α signaling, and not because of general cytotoxicity. The discrepancy between *in vitro* and *in vivo* tumor cell response to PT2385 may be attributed to the ability of *in vitro* growth medium to allow the cells to become independent of HIF2 α signaling.

Another discrepancy between *in vitro* and *in vivo* effects of HIF2 α antagonism involves HIF2 α levels. In excised 786-O tumors after PT2385 treatment, both tumor HIF2 α mRNA and protein are decreased in a dose-dependent manner (Fig. 4D and E). Neither is diminished in cell culture (Supplementary Fig. S4). Previous research suggests that HIF2 α regulates its transcription (31, 32), supporting that the reduction of HIF2 α observed *in vivo* after PT2385 treatment is the result of inhibition of transcription. However, at this time, we cannot rule out that HIF2 α /ARNT heterodimerization disruption with PT2385 treatment results in increased HIF2 α protein instability. Regardless of the precise mechanism, the effect of PT2385 on HIF2 α target gene inhibition appears to be the result of both inhibition of HIF2 α transcriptional activity and reduction of HIF2 α protein levels. As appears to also be the case in cell proliferation experiments, *in vitro* cell culture

conditions may diminish the putative role of HIF2 α . Not surprisingly, these data suggest that *in vitro* conditions appear unsuitable to study the tumor microenvironment effects of hypoxia signaling.

The HIF2 α protein does not accumulate in the majority of normal adult tissues due to its restricted expression pattern and tight posttranslational control. The limited role of HIF2 α in normal adult physiology suggests that as therapeutics, specific HIF2 α antagonists may have few side effects. In rodents, under all conditions tested herein, PT2385 is well tolerated, with no weight loss or behavioral changes observed. Importantly, treatment of xenograft tumor-bearing mice with PT2385 represses circulating tumor-derived human VEGF-A levels but has no effect on levels of host VEGF-A (Fig. 6B and C). In addition to its control of multiple tumorigenic gene products, specific inhibition of tumor-derived VEGF-A inhibition distinguishes HIF2 α antagonists from the currently approved antiangiogenic therapies whose systemic angiogenesis inhibition leads to cardiovascular safety concerns. In particular, hypertension is one of the most frequently observed adverse effects in patients treated with anti-VEGF therapy and can often be dose limiting (34, 38). Under conditions in which sunitinib causes a large increase in blood pressure in rats, no change is observed with PT2385 treatment (Fig. 6A). The lack of hypertension coupled with tumor regression without any adverse events in preclinical models suggests that HIF2 α antagonism with PT2385 may provide patients afflicted with ccRCC, a novel therapeutic option with an exceptional safety profile. As such, clinical evaluation of PT2385 for the treatment of kidney cancer is ongoing.

Disclosure of Potential Conflicts of Interest

No potential conflicts of interest were disclosed.

Authors' Contributions

Conception and design: E.M. Wallace, J.P. Rizzi, G. Han, P.M. Wehn, Z. Cao, J.A. Grina, S.T. Schlachter, H. Tan, B. Wang, R. Xu, J.A. Josey

Development of methodology: Z. Cao, X. Du, T. Cheng, H. Tan, B. Wang, S. Xie, R. Xu, H. Yang

Acquisition of data (provided animals, acquired and managed patients, provided facilities, etc.): G. Han, Z. Cao, X. Du, T. Cheng, R.M. Czerwinski, B.S. Goggin, M.M. Halfmann, M.A. Maddie, H. Tan, K. Wang, S. Xie, R. Xu
Analysis and interpretation of data (e.g., statistical analysis, biostatistics, computational analysis): E.M. Wallace, J.P. Rizzi, G. Han, Z. Cao, X. Du, T. Cheng, D.D. Dixon, B.S. Goggin, M.M. Halfmann, S.R. Olive, H. Tan, K. Wang, S. Xie, R. Xu

Writing, review, and/or revision of the manuscript: E.M. Wallace, J.P. Rizzi, G. Han, Z. Cao, X. Du, D.D. Dixon, R. Xu, J.A. Josey

Administrative, technical, or material support (i.e., reporting or organizing data, constructing databases): J.P. Rizzi, D.D. Dixon, B.S. Goggin, M.M. Halfmann, S.R. Olive

Study supervision: E.M. Wallace, G. Han, Z. Cao, J.A. Josey

Grant Support

This work was supported in part by Cancer Prevention and Research Institute of Texas (all authors).

The costs of publication of this article were defrayed in part by the payment of page charges. This article must therefore be hereby marked *advertisement* in accordance with 18 U.S.C. Section 1734 solely to indicate this fact.

Received February 22, 2016; revised June 19, 2016; accepted July 6, 2016; published OnlineFirst September 6, 2016.

References

- American Cancer Society. Kidney cancer (adult) – renal cell carcinoma. Atlanta, GA: American Cancer Society; 2014.
- Sosman J, Puzanov I. Combination targeted therapy in advanced renal cell carcinoma. *Cancer* 2009;115:2368–75.
- Wang GL, Jiang BH, Rue EA, Semenza GL. Hypoxia-inducible factor 1 is a basic-helix-loop-helix-PAS heterodimer regulated by cellular O₂ tension. *Proc Natl Acad Sci USA* 1995;92:5510–14.
- Tian H, McKnight SL, Russell DW. Endothelial PAS domain protein 1 (EPAS1), a transcription factor selectively expressed in endothelial cells. *Genes Dev* 1997;11:72–82.
- Gu YZ, Moran SM, Hogenesch JB, Wartman L, Bradfield CA. Molecular characterization and chromosomal localization of a third alpha-class hypoxia inducible factor subunit, HIF3alpha. *Gene Expr* 1998;7:205–13.
- Kaelin WJ, Ratcliffe PJ. Oxygen sensing by metazoans: the central role of the HIF hydroxylase pathway. *Mol Cell* 2008;30:393–402.
- Majmundar AJ, Wong WJ, Simon MC. Hypoxia-inducible factors and the response to hypoxic stress. *Mol Cell* 2010;40:294–309.
- Keith B, Johnson RS, Simon MC. HIF1 α and HIF2 α : sibling rivalry in hypoxic tumour growth and progression. *Nat Rev Cancer* 2011;12:9–22.
- Jaakkola P, Mole DR, Tian YM, Wilson MI, Gielbert J, Gaskell SJ, et al. Targeting of HIF- α to the von Hippel-Lindau ubiquitylation complex by O₂-regulated prolyl hydroxylation. *Science* 2001;292:468–472.
- Bruick RK, McKnight SL. A conserved family of prolyl-4-hydroxylases that modify HIF. *Science* 2001;294:1337–40.
- Sato Y, Yoshizato T, Shiraishi Y, Maekawa S, Okuno Y, Kamura T, et al. Integrated molecular analysis of clear-cell renal cell carcinoma. *Nat Genet* 2013;45:860–7.
- Kondo K, Klco J, Nakamura E, Lechpammer M, Kaelin WJ. Inhibition of HIF is necessary for tumor suppression by the von Hippel-Lindau protein. *Cancer Cell* 2002;1:237–46.
- Maranchie JK, Vasselli JR, Riss J, Bonifacino JS, Linehan WM, Klausner RD. The contribution of VHL substrate binding and HIF1- α to the phenotype of VHL loss in renal cell carcinoma. *Cancer Cell* 2002;1:247–55.
- Kondo K, Kim WY, Lechpammer M, Kaelin WJ. Inhibition of HIF2 α is sufficient to suppress pVHL-defective tumor growth. *PLoS Biol* 2003;1:E83.
- Zimmer M, Doucette D, Siddiqui N, Iliopoulos O. Inhibition of hypoxia-inducible factor is sufficient for growth suppression of VHL-/- tumors. *Mol Cancer Res* 2004;2:89–95.
- Monzon FA, Alvarez K, Peterson L, Truong L, Amato RJ, Hernandez-McClain J, et al. Chromosome 14q loss defines a molecular subtype of clear-cell renal cell carcinoma associated with poor prognosis. *Mod Pathol* 2011;24:1470–9.
- Shen C, Beroukhi R, Schumacher SE, Zhou J, Chang M, Signoretti S, et al. Genetic and functional studies implicate HIF1 α as a 14q kidney cancer suppressor gene. *Cancer Discov* 2011;1:222–35.
- Rogers JL, Bayeh L, Scheuermann TH, Longgood J, Key J, Naidoo J, et al. Development of inhibitors of the PAS-B domain of the HIF-2 α transcription factor. *J Med Chem* 2013;56:1739–47.
- Scheuermann TH, Li Q, Ma HW, Key J, Zhang L, Chen R, et al. Allosteric inhibition of hypoxia inducible factor-2 with small molecules. *Nat Chem Biol* 2013;9:271–6.
- Scheuermann TH, Tomchick DR, Machius M, Guo Y, Bruick RK, Gardner KH. Artificial ligand binding within the HIF2 α PAS-B domain of the HIF2 transcription factor. *Proc Natl Acad Sci USA* 2009;106:450–5.
- Otwinowski Z, Minor W. Processing of X-ray diffraction data collected in oscillation mode. *Methods Enzymol* 1997;276:307–26.
- Emsley P, Cowtan K. Coot: model-building tools for molecular graphics. *Acta Crystallogr D Biol Crystallogr* 2004;60:2126–32.
- Murshudov GN, Vagin AA, Dodson EJ. Refinement of macromolecular structures by the maximum-likelihood method. *Acta Crystallogr D Biol Crystallogr* 1997;53:240–55.
- Key J, Scheuermann TH, Anderson PC, Daggett V, Gardner KH. Principles of ligand binding within a completely buried cavity in HIF2 α PAS-B. *J Am Chem Soc* 2009;132:17647–54.
- Wu D, Potluri N, Lu J, Kim Y, Rastinejad F. Structural integration in hypoxia-inducible factors. *Nature* 2015;524:303–8.
- Gruber M, Hu CJ, Johnson RS, Brown EJ, Keith B, Simon MC. Acute postnatal ablation of Hif-2 α results in anemia. *Proc Natl Acad Sci USA* 2007;104:2301–6.
- Rankin EB, Biju MP, Liu Q, Unger TL, Rha J, Johnson RS, et al. Hypoxia-inducible factor-2 (HIF-2) regulates hepatic erythropoietin *in vivo*. *J Clin Invest* 2007;117:1068–77.
- Nakamura E, Abreu-e-Lima P, Awakura Y, Inoue T, Kamoto T, Ogawa O, et al. Clusterin is a secreted marker for a hypoxia-inducible factor-independent function of the von hippel-lindau tumor suppressor protein. *Am J Pathol* 2006;168:574–84.
- Hu C-J, Wang L-Y, Chodosh LA, Keith B, Simon MC. Differential roles of hypoxia-inducible factor 1 α (hif-1 α) and hif-2 α in hypoxic gene regulation. *Mol Cell Biol* 2003;23:9361–74.
- Kim WY, Safran M, Buckley MR, Ebert BL, Glickman J, Bosenberg M, et al. Failure to prolyl hydroxylate hypoxia-inducible factor α phenocopies VHL inactivation *in vivo*. *EMBO J* 2006;25:4650–62.
- Sato M, Tanaka T, Maeno T, Sando Y, Suga T, Maeno Y, et al. Inducible expression of endothelial pas domain protein-1 by hypoxia in human lung adenocarcinoma A549 cells role of src family kinases-dependent pathway. *Am J Respir Cell Mol Biol* 2002;26:127–34.
- Gordan JD, Lal P, Dondeti VR, Letrero R, Parekh KN, Oquendo CE, et al. HIF- α effects on c-Myc distinguish two subtypes of sporadic VHL-deficient clear cell renal carcinoma. *Cancer Cell* 2008;14:435–46.
- Kamba T, McDonald DM. Mechanisms of adverse effects of anti-VEGF therapy for cancer. *Br J Cancer* 2007;96:1788–1795.
- Hamnvik OP, Choueiri TK, Turchin A, McKay RR, Goyal L, Davis M, et al. Clinical risk factors for the development of hypertension in patients treated with inhibitors of the VEGF signaling pathway. *Cancer* 2015;121:311–9.
- Facemire CS, Nixon AB, Griffiths R, Hurwitz H, Coffman TM. Vascular endothelial growth factor receptor 2 (vegfr2) controls blood pressure by regulating nitric oxide synthase expression. *Hypertension* 2009;54:652–8.
- Kappers MHW, van Esch JHM, Sluiter W, Sleijfer S, Danser AHJ, van den Meiracker AH. Hypertension induced by the tyrosine kinase inhibitor sunitinib is associated with increased circulating endothelin-1 levels. *Hypertension* 2010;56:675–81.
- Shen C, Kaelin WG. The VHL/HIF axis in clear cell renal carcinoma. *Semin Cancer Biol* 2013;23:18–25.
- Jain RK, Duda DG, Clark JW, Loeffler JS. Lessons from phase III clinical trials on anti-VEGF therapy for cancer. *Nat Clin Pract Oncol* 2006;3:24–40.